Structural Engineering and Mechanics, *Vol. 74, No. 6 (2020) 789-807*
DOI: https://doi.org/10.12989/sem.2020.74.6.789

Non-linear dynamic assessment of low-rise RC building model under sequential ground motions

Syed Muhammad Bilal Haider[1], Zafarullah Nizamani*[1] and Chun Chieh Yip[2]

[1]Department of Environmental Engineering, Universiti Tunku Abdul Rahman, 31900 Kampar, Malaysia
[2]Department of Civil Engineering, Universiti Tunku Abdul Rahman, 43000 Kajang, Malaysia

(Received August 12, 2019, Revised January 23, 2020, Accepted February 4, 2020)

Abstract. Multiple earthquakes that occur during short seismic intervals affect the inelastic behavior of the structures. Sequential ground motions against the single earthquake event cause the building structure to face loss in stiffness and its strength. Although, numerous research studies had been conducted in this research area but still significant limitations exist such as: 1) use of traditional design procedure which usually considers single seismic excitation; 2) selecting a seismic excitation data based on earthquake events occurred at another place and time. Therefore, it is important to study the effects of successive ground motions on the framed structures. The objective of this study is to overcome the aforementioned limitations through testing a two storey RC building structural model scaled down to 1/10 ratio through a similitude relation. The scaled model is examined using a shaking table. Thereafter, the experimental model results are validated with simulated results using ETABS software. The test framed specimen is subjected to sequential five artificial and four real-time earthquake motions. Dynamic response history analysis has been conducted to investigate the i) observed response and crack pattern; ii) maximum displacement; iii) residual displacement; iv) Interstorey drift ratio and damage limitation. The results of the study conclude that the low-rise building model has ability to resist successive artificial ground motion from its strength. Sequential artificial ground motions cause the framed structure to displace each storey twice in correlation with vary first artificial seismic vibration. The displacement parameters showed that real-time successive ground motions have a limited impact on the low-rise reinforced concrete model. The finding shows that traditional seismic design EC8 requires to reconsider the traditional design procedure.

Keywords: time history analysis; reinforced concrete framed structure; sequential ground motions; shaking table; ETABS; Buckingham π theorem

1. Introduction

There is an increase in trend towards the use of performance based design method however Malaysia is still progressing towards adopting such design methodology. The evolution process from traditional earthquake design to Performance Based Earthquake Engineering (PBEE) methodology provides an effective sustainable design tool. PBEE investigates the events from past to recent seismic excitations and helps to improve ground motion risk decision making to form a comprehensive design and better assessment procedure (Moehle and Deierlein 2004). In order to utilize PBEE effectively and intelligently, Malaysian reinforced concrete (RC) structures required such a design code which allows structure sustainability and resiliency against multiple ground motions. Therefore, sustainable building is considered as a way for the construction industry to resolve environmental, social and economic issues (Akadiri *et al.* 2012).

According to Malaysian National Annex (MS EN 1998-1 2015), Malaysia is located in a low seismic zone. However, still, 11 out of 13 states follow British Standard BS8110 code, a code that does not include any condition for earthquakes (Megawati *et al.* 2004). Usually, first seismic excitation (main shock) followed by another seismic motion (after-shock) within a few hours which may recur again for next few days. Surprisingly, in the current situation, the provisions recommended by FEMA368 (2000) and Eurocode 8 (2004) ignore the repetition of seismic vibration in the analysis (Adiyanto and Majid 2014; Moustafa and Takewaki 2011). Amadio *et al.* (2003) has proved that repeated seismic excitations affected the strength of the building and hence, required to over-strength the building after each seismic motion. Repeated seismic motions produced 1.3 to 1.4 times increment in the maximum storey ductility as compared with single seismic event (Faisal *et al.* 2013; Hatzivassiliou and Hatzigeorgiou 2015). Thus, traditional structural design code i.e. EC8 needs to be revised, incorporating the procedures of multiple ground motions (Amadio *et al.* 2003, Faisal *et al.* 2013). Moreover, a research study was required which particularly focused on Malaysian RC structures reconsidering the traditional design code (Eurocode 8 2004) in accordance with Malaysia National Annex to MS EN 1998-1 (2015) for multiple excitations.

Nonlinear time history also termed as real-time ground motion verifies the expected seismic performance of a structural model. In Malaysia, due to the activation of regional fault lines (Abas *et al.* 2017), local ground motions have been recorded since the year 2007 (Marto and Kasim

*Corresponding author, Ph.D.
E-mail: zafarullah@utar.edu.my

http://www.techno-press.com/journals/sem&subpage=7
ISSN: 1225-4568 (Print), 1598-6217 (Online)

2013). Adiyanto and Majid (2014) reported that most of the buildings in Peninsula Malaysia were going through concrete deterioration due to multiple seismic ground movements from near and far field. According to Seismological Division of Malaysian Meteorological Service, Sumatran subduction zone (Indian and Eurasian plates overlap) had potential to produce the future giant earthquake of moment magnitude of about 9.0 (Mw) (Abas 2001). However up-to-date, intensive real-time local earthquake have not been observed in Malaysia therefore, artificially produced intensive harmonic waves can be produced and used to assess the Malaysian RC structures. According to the best of authors' knowledge, the most common limitation in all past studies is that they have selected such real-time ground motion events which were held and recorded in other locations and different time period. Moreover, the effect of artificially produced harmonic seismic vibration required to take into account. Additionally, in Malaysia, all the past studies have focused on analyzing the structure using simulation only and no experimental work had been performed to investigate the framed structures.

In the light of the above discussion, a regular two storey reinforced concrete (RC) structural model is designed, constructed and investigated under a series of five artificial and four real-time earthquake motions. For this objective, the prototype full-scale model is scaled down by 1:10 through a similitude method i.e. Buckingham π Theorem. Thereafter, the building model is assessed on a shaking table for consecutive five artificial ground motions. The results are validated with finite element commercial software ETABS which examines the full-scale model through nonlinear dynamic time history analysis along with five artificial and three real-time seismic excitations. The most critical parameters of building response determined are observed cracks, maximum displacement, residual displacement, interstorey drift ratio, and damage limitation.

2. Literature review

In order to better understand the nonlinear dynamic behavior of RC structures against multiple excitation, research studies were conducted to derive expressions for the damage features and displacement response. Models of single degree of freedom (SDOF) and multiple degree of freedom (MDOF) systems have been developed and widely used in literature.

In the past decades, studies reported that the repeated earthquake ground motions have a significant impact on framed structures. Hatzivassiliou and Hatzigeorgiou (2015) investigated the behavior of three-dimensional RC structures under multiple earthquakes. Their study substantiated that multiple earthquakes lead to accumulating structural damage. Khoshraftar *et al.* 2013) concluded that 40% degradation of strength or 50% degradation of stiffness caused severe structural damage in the RC buildings. It was further determined that strength degradation had more influence on increasing the damage index in comparison with stiffness degradation.

Few studies highlighted the seismic impact on Malaysian RC structures. For example, Ismail *et al.* (2017) studied the vulnerability of public buildings subjected to earthquake event to assess the performance of two critical frame reinforced concrete buildings. Their study indicated that no structural failure was recorded due to both buildings damage index less than 1.0. All beams formed plastic hinges earlier than columns. Another study was conducted to assess the vulnerability of three reinforced concrete public buildings located in Ipoh, Malaysia (Ismail and Adnan 2016). The buildings were analyzed using finite element modeling software IDARC under a variety of earthquake intensities from Time History Analysis (THA) considering low to medium earthquake intensities. Results identified that medium rise building had light damage level with a damage index of 0.032 at an earthquake intensity of 0.15 g however, high rise building had damage index in the range 0.050 (light damage level) to 1.0 (collapse) at earthquake intensity of 0.05 g. The columns showed light damages whereas beams were in much critical conditions, the distribution of the damage index reflected the seismic design principle of "strong column, weak beam". Ismail *et al.* (2016) addressed the performance of high rise building present in Malaysia by simulating the four building models. Results concluded that if peak ground acceleration reached 1g a complete collapse occurred in the building model. Another simulation study for the damage assessment was conducted with six reinforced concrete buildings categorized as medium-rise moment resisting frames (Ismail *et al.* 2018). In this study a variation of low earthquake intensities (0.05g, 0.10g, 0.15g, 0.2g) were assessed. Their study declared that even at maximum earthquake motion of 0.2g, there was no structural damage. One more study was conducted to evaluate low-intensity earthquakes effects on high rise building in Kedah, Malaysia (Ismail and Zamahidi 2015). Simulation results showed that the building failure started by yielding of a beam at 3.115sec and at an intensity of 0.20 g however there was no structural collapse. Ismail *et al.* (2014) simulated medium rise four storey college building located in Johar, Malaysia with a low intensity earthquake excitation. At 0.15g, initial yielding started in the beam at 4.265 sec in storey 2 however, building model survive till 0.2g and there was no structural failure recorded. A study addressed a vertical geometric irregularity frame structures of seven storey building located in Selangor, Malaysia (Rozaina 2018). A reinforced concrete building model was investigated using Ranau earthquake seismic vibrations to check the soft storey and the appearance of sequence of the plastic hinges during sequential ground motions (Tan *et al.* 2017). Their study showed that the soft storey structure had the lowest seismic resistance and collapsed at 0.55g. Plastic hinge propagation was dominant at the soft storey columns which made building susceptible under earthquake loading. An experimental study had been conducted on four RC two storey residential building models (Bahadir and Balik 2018). The experiential models were scaled to 1/6 and placed at different angles on the Shaking table to examine the structural behaviour. Multiple ground motions were applied until the structural failure occurred. The results showed that each model had a soft storey that is 1st storey which was completely destroyed at the end of each test. Column beam and column base were the most critical joints where plastic hinges produced in each test. Another study was conducted on one storey, two full scale RC building models placed on shaking table (Bayhan 2013). Simulated models were also drawn to assess the seismic response. Models were subjected to four consecutive shaking table motions with increasing intensity from 0.05g to 0.53g. Their study obtained appropriate modeling and computing techniques with reference to the shaking table tests results.

Displacement response is a critical parameter and plays a vital role in earthquake assessment, therefore, EC8 suggested that interstorey drift ratio (IDR) act as a verification criterion for damage limitation (EC8 clause 4.4.3.1(1) and 4.4.3.2(1)). The limit set on the interstorey drift ratio for no collapse requirement is 1% if there are no nonstructural elements attached to the structure. Oyguc *et al.* (2018) proof that interstorey drifts worked as an effective damage control measure. Their study also acknowledged that in some cases, the aftershocks did not increase the residual displacements too. Yaghmaei-Sabegh and Ruiz-García (2016) evaluated the inelastic displacement and strength demands under seismic sequence. Yaghmaei-Sabegh *et al.* (2017) also examined the seven approximate methods to estimate maximum roof displacements and maximum interstorey drift ratios of multi-degree-of-freedom (MDOF) systems. Ruiz-García *et al.* (2018) examined the response of three-dimensional (3-D) steel moment-resisting buildings having 3, 9, and 20 storey height under bi-directional attack of real seismic sequences. Their study concluded the results in terms of lateral interstory drift demands. Yaghmaei-Sabegh and Mahdipour-Moghanni (2019) studied the state dependent fragility curves using real and artificial earthquake sequences. Samanta and Pandey (2018) examined the effects of ground motion duration on the seismic performance of a building. Their study showed that the maximum story drift ratio was not affected by ground motion duration. The residual drift or the permanent deformation of the building after each seismic event are measured and used to infer the degree of sustained damage to the building. Residual drift has been evaluated in past studies. Manafpour and Moghaddam (2019) had described the response of a reinforced concrete SDOF system subjected to different orders of near- and far-field records in multiple earthquakes. The performance evaluation is carried out for various first shock damage levels and second shock performance levels. Their study highlights the fact that increment of relative intensity level in the second shock had maximum influence on the residual drift as compared to the first shock. Hosseinpour and Abdelnaby (2017) identified that changing the earthquake direction affects the total drift demands and number of plastic hinges and caused maximum total residual drifts in the framed structure.

Use of zero padding and baseline correction technique makes cosine Fourier transform methodology very effective. A shaking table test was performed to verify the conversion methods for acceleration and displacement data (Heuisoo *et al.* 2019). A small scaled 10 storey building model was attached with contact sensor accelerometers and high-speed images to record the data under strong ground motions. In their study, data recorded by accelerometers were validated with high speed images, thereafter, three different methods were used to correct and convert acceleration into velocity and displacement. Their study revealed that cosine Fourier transform and baseline correction are the most suitable method to process the data. The converted displacement obtained from such method was close to data recorded by shaking table.

3. Description of structure and experimental details

3.1 Similitude relation

Geometrical scaled models are promoted instead of full-scale models to save time as well as money. Dimensional analysis is a technique which is used to make a similitude relationship between the models. In order to have a cost-efficient model, dimensional analysis method provides a similitude between the prototype and scaled model. Moreover, dimensional analysis uses Buckingham π Theorem to create a relationship of geometry, loads and material properties among the models (Rastogi *et al.* 2015). Buckingham π Theorem concludes that independent Pi's of the model (m) should have similitude relationship with the corresponding independent Pi's of the prototype model (p) as shown in Eq. (1),

$$\pi_{model\ (m)} = \pi_{prototype\ (p)} \tag{1}$$

In this study, 10 physical parameters have been selected to make a relationship between the scale down and prototype model. All the selected variables are based on geometrical and material properties of the model and their parameters in functional form (Rastogi *et al.* 2015) as shown in Eq. (2).

$$\sigma = f\,(d,\ t,\ \rho,\ E,\ g,\ l,\ V,\ \Omega,\ v) \tag{2}$$

Where, σ = stress, d = displacement, t = time, ρ = density, E = modulus of elasticity, g = spectral acceleration, l = length, V = shear force, Ω = frequency, and v = velocity.

Here, Eq. (2) shows that stress σ is a dependent variable and remaining parameters are independent variable. As E, ρ, and l are repeating variables models (Rastogi *et al.* 2015), therefore, one equation would be derived by multiplying dependent variable (σ) with the product of repeating variables (E, ρ, and l) to form a dimensionless group π_1. Moreover, six equations would be formed by multiplying each independent variable (d, t, g, V, Ω, v) one by one with the product of repeating variables (E, ρ, and l) forming dimensionless group π_2 to π_7. Thus, seven equations are derived as shown in Eq. 3 and 4.

$$\{\pi_r\}=\{(\pi_1)_r,\ (\pi_2)_r,\ (\pi_3)_r,\ (\pi_4)_r,\ (\pi_5)_r,\ (\pi_6)_r,\ (\pi_7)_r \tag{3}$$

or

$$\{\pi_r\}=\left\{\left(\frac{\sigma}{E}\right)_r, \left(\frac{d}{l}\right)_r, \left(\frac{t}{l}\sqrt{\frac{E}{\rho}}\right)_r, \left(\frac{g\rho l}{E}\right)_r, \left(\frac{V}{E}\right)_r, \left(\Omega l\sqrt{\frac{\rho}{E}}\right)_r, \left(\frac{v\rho l}{E}\right)_r\right\} \quad (4)$$

$$S_E = (m_p / m_m) \, . \, S_a \, . \, (1/S^2)$$

3.1.2 Similitude requirement

The four dimensionless terms derived must be equal for the model and the prototype in order to match the functional relationship between them as shown in Eq. (1). The first dimensionless term $\pi_{1model} = \pi_{1prototype}$ i.e.,

$$\frac{\sigma_m}{E_m} = \frac{\sigma_p}{E_p}$$

$$\frac{E_p}{E_m} = \frac{\sigma_p}{\sigma_m} \quad (5)$$

$$\sigma_m = \frac{\sigma_p}{S_E}$$

Where, $S_E = \frac{E_P}{E_m}$, the dimensional scaling factor. S_E is the ratio of modulus of elasticity of the prototype to that of the model. From Eq. (5), it follows that the model stress is scale factor *'S_E'* times lesser the stress in the prototype. Similarly, for Eq. (6), the second dimensionless term is represented as,

$$\frac{d_m}{l_m} = \frac{d_p}{l_p}$$

$$\frac{l_p}{l_m} = \frac{d_p}{d_m} \quad (6)$$

$$d_m = \frac{d_p}{S}$$

Where $S = \frac{l_p}{l_m}$ is the dimensional scale factor.

3.1.3 Calculation of scaling factor 'S_E'

From Eq. (5), S_E is derived as shown in Eq. (7),

$$S_E = E_p / E_m \quad (7)$$

As we know that $E = F/L^2$, so substitute in Eq. (7) to get Eq. (8) as,

$$S_E = F_p L_m^2 / L_p^2 F_m \quad (8)$$

Substitute $F = ma$ in Eq. (8),

$$S_E = (m_p \, . \, a_p \, . \, L_m^2)/(L_p^2 \, . \, m_m \, . \, a_m)1$$

Rearrange the values,

$$S_E = (m_p / m_m) \, . \, (a_p/a_m) \, . \, (l_m^2/l_p^2)$$

Substitute $a_p/a_m = S_a$ *and* $l_p/l_m = S$,

Here, Eq. (9) shows the derived equation of S_E to calculate the scaling factor.

$$S_E = (m_p / m_m) \, . \, S_a \, . \, (1/S^2) \quad (9)$$

3.1.4 Theoretical mass of column

As the equation of S_E has been derived, select one column out of eight columns from the prototype full scale model to get the theoretical mass of each column.

Volume of Column = Length × Breadth × Height

Volume of Column = 600mm × 400mm × 7000mm

Volume of Column = 1.68m^3

Mass of Prototype (column) = Density of Concrete × Volume

Mass of Prototype (column) = 2500 × 1.68

Mass of Prototype (column)= 4200kg

So, the theoretical mass of each prototype full scale column is 4200kg.

3.1.5 Mass of actual experimental column

The fabrication process of the column is shown in Fig. 1. To calculate the actual mass of small scaled column, construct a column and get the weight of it.

Measured Mass of small scale column = 4.22kg

Now, consider the Eq. (9) to calculate S_E,

$$S_E = (4200/4.22) \times 1 \times (1 / 10^2)$$

$$S_E = 9.9$$

Here, Table 1 shows the different similitude relationships and scale factors for the dynamic structural model.

Table 1 Similitude relation between prototype and scaled model

Parameters	Dimensions	Scale Factor	
		Variables	1:10 Scale down model
Modulus, E	FL^{-2}	S_E	9.9
Stress, σ	FL^{-2}	S_E	9.9
Acceleration, a	LT^{-2}	1	1
Length, l	L	S	10
Point load, P	F	$S_E S^2$	$9.9 \times (10)^2$
Time, t	T	$S^{1/2}$	$(10)^{1/2}$
Frequency, Ω	T^{-1}	$S^{-1/2}$	$(10)^{-1/2}$
Velocity, v	LT^{-1}	$S^{1/2}$	$(10)^{1/2}$

Fig. 1 Small scale column

Table 2 Variables of structural model

Standard deviation:	
f_c	0.95
f_y (ϕ1.6mm, and ϕ3.2mm)	1.33, and 1.39
Variance:	
f_c	0.91
f_y	1.76, and 1.69
General specifications:	
W/C ratio	0.42
Poison ratio	0.18
Beam dimension (Length × width)	60mm × 25mm
Column dimension (Length × width)	60mm × 40mm
Slab thickness	16mm

Table 3 Reinforcement strength details

Reinforcement bar (mm)	Average yield stress (MPa)	Average modulus of elasticity (GPa)
1.6	540.95	144.02
3.2	504.95	160.56

3.2 Specimen specifications

A small scaled reinforced concrete building model that is actually a prototype of a segment of Block N, Universiti Tunku Abdul Rahman (UTAR), Malaysia is examined in this study. The building model has two storey and rectangular in shape The labeled three dimensional scaled model is shown in Fig. 3. The experimental model is scaled (Yip *et al.* 2018) to 1/10 having 3 bay on X-axis and 1 bay on the Y-axis. Moreover, Malaysia has been considered as low seismic zone (Sooria *et al.* 2012) therefore, a low-rise frame structure is constructed following the guidelines of Eurocode 2 (2004) and Eurocode 8 (2004) for Ductility Class Low (DCL). Details of test specimen is shown in Table 2.

3.3 Reinforcement specification

In this study, reinforcement has been calculated manually based on Eurocode 2 (2004) and Eurocode 8 (2004) guidelines. Main reinforcement bars of beams and columns used 3.2mm diameter of bars however, shear rings and ties used 1.6mm diameter of the bar. In both prototype and scaled models, beams and columns have an identical rectangular cross-section in each storey. Moreover, intermediate beams are placed and located only in the 1st and 2nd story. Here, Fig. 2 shows the complete details of the reinforcement of scaled model.

Moreover, Fig. 4 showed the reinforcement detail of footing and fixing of the frame structure on shaking table. The dimension of footing is 100mm×200mm×40mm. The footing of the experimental model was connected with base of plywood through bolt connection. This plywood plate was fixed on the top shaking table plate and it worked as a connecting layer between the footing and the shaking table.

The model has eight columns and two storeys. Here, Fig. 5 illustrates the beam column joint detailed reinforcement of a corner column of the framed structure.

In this study, tensile tests were conducted for six sample bars each with a diameter 1.6mm and 3.2mm in Mechanical laboratory of Universiti Tunku Abdul Rahman, Malaysia. The average yield stress and modulus of elasticity recorded for each sample bar is shown in Table 3.

Fig. 6 showed the stress strain curve for ϕ1.6mm and ϕ3.2mm bar respectively. In ϕ1.6mm bar, the deformation was started with gentle elongation and yield stress at 0.0055mm and 541.21 MPa as shown in Fig. 6 (a).

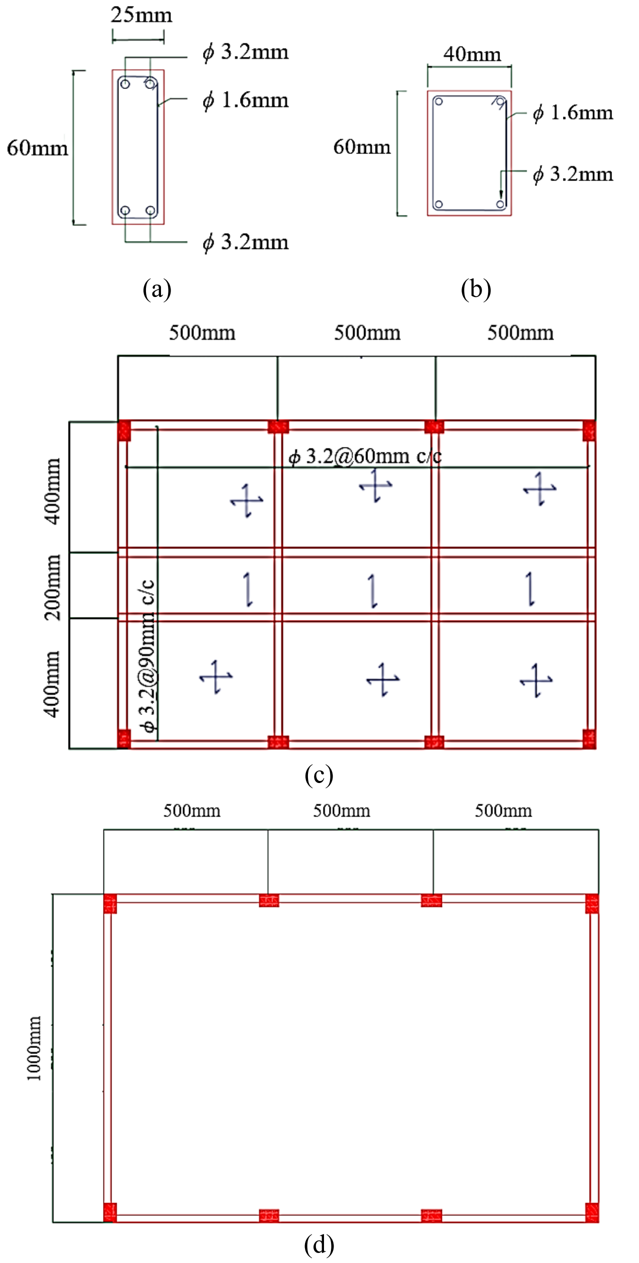

Fig. 2 Experimental model geometry and reinforcement details (a) Beam Reinforcement details; (b) Column Reinforcement details; (c) 1st and 2nd storey Slab reinforcement and Plan layout; (d) Base Plan layout

Fig. 3 Labeled Geometry and Elevation of RC frame building model

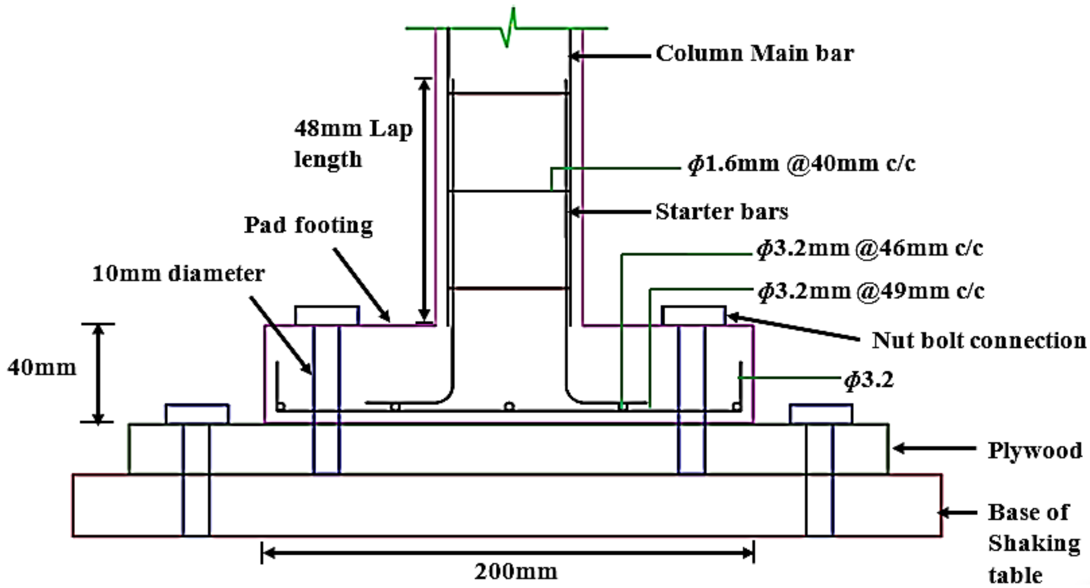

Fig. 4 Footing reinforcement detail and fixing of the test specimen on shaking table

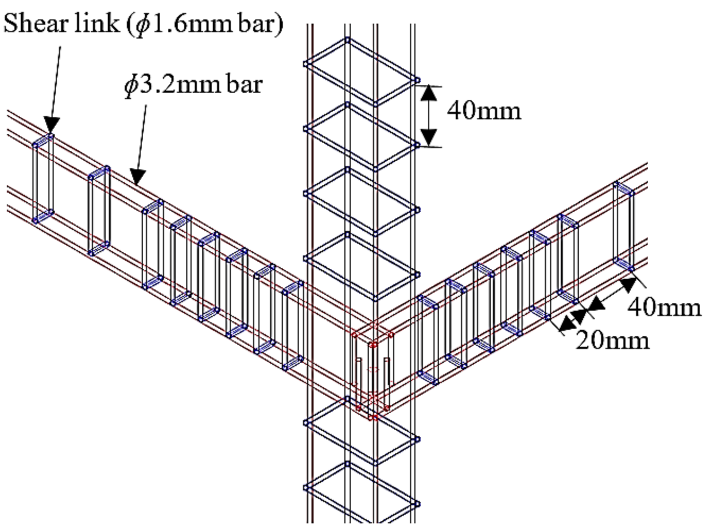

Fig. 5 Beam Column joint connection at each storey level

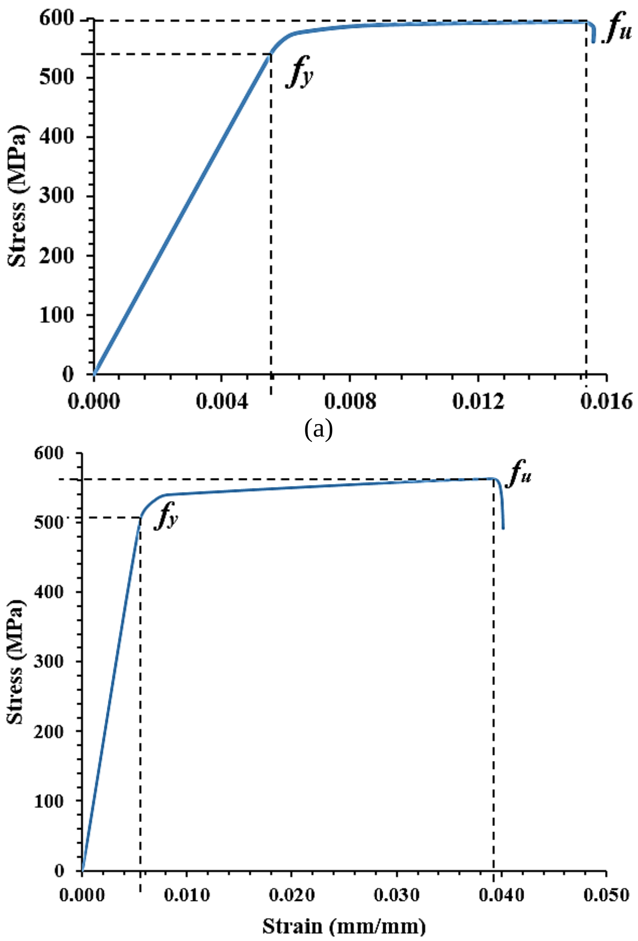

Fig. 6 Stress strain diagram of typical reinforcing steel bar (a) 1.6mm; (b) 3.2mm

Table 4 Concrete Mix Design Components

Cement (kg/m^3)	Water (kg/m^3)	Fine aggregate (kg)	Coarse aggregate (kg)	Water / cement ratio	Density (kg/m^3)	Admixture 1.2% , (kg)
550.0	233.0	511.0	1086.0	0.42	2380	6.6

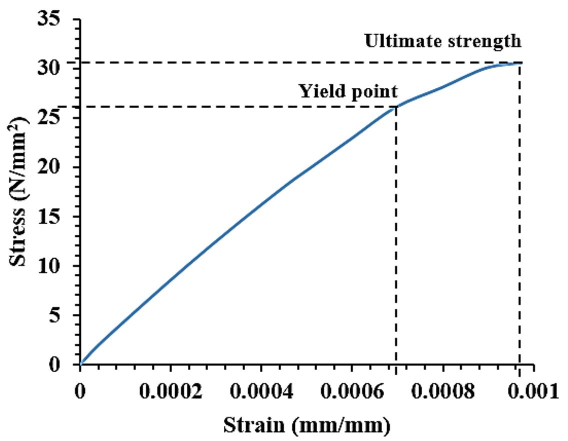

Fig. 7 Stress strain diagram of concrete grade 30

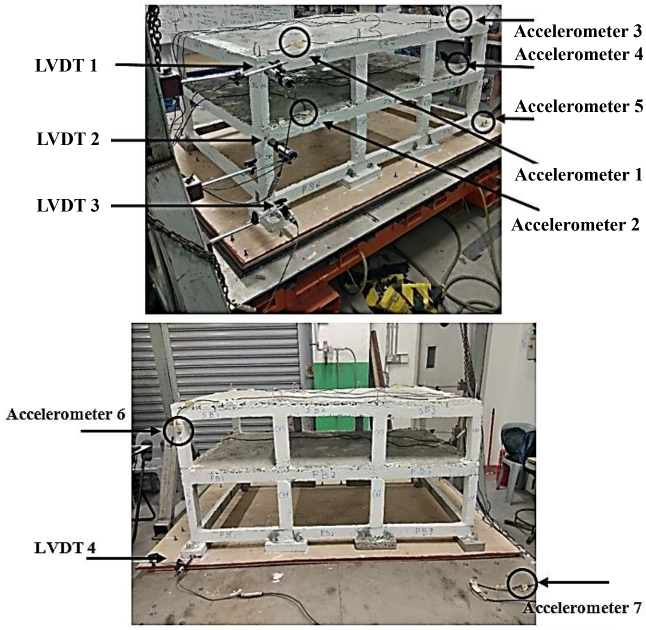

Fig. 8 Schematic placement and arrangement of Accelerometers and LVDT

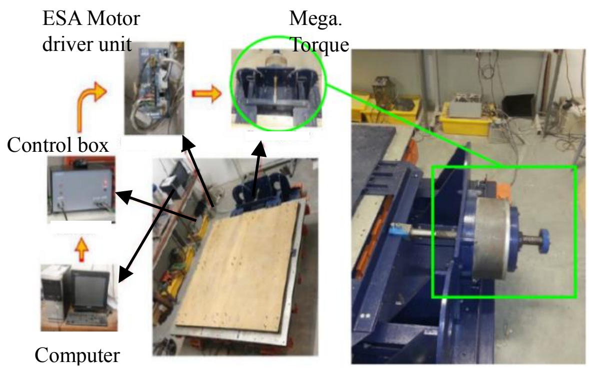

Fig. 9 Shaking Table system

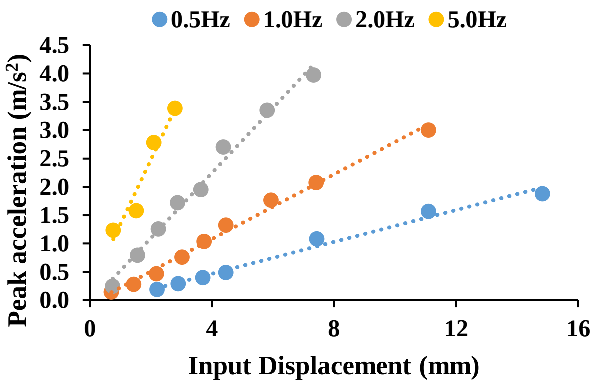

Fig. 10 The relationship between the input linear displacement and the measured peak acceleration in shaking table (Lim *et al.* 2018)

Thereafter, the curve eventually showed the maximum strain and stress at 0.0153mm and 594.15MPa respectively. Similarly, Fig. 6 (b) illustrated that the ϕ3.2mm bar starts to deform at 0.0055mm with a yield stress 504.06MPa. The maximum strain and stress found from the curve is 0.0392mm and 562.62MPa as shown in Fig. 6 (b).

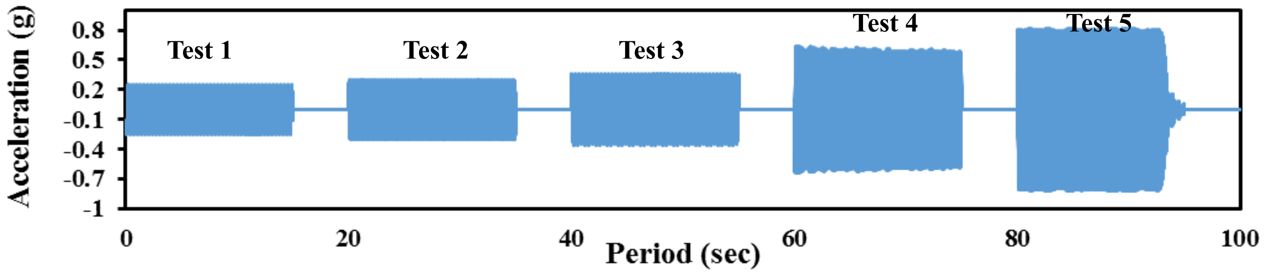

Fig. 11 (a) Input acceleration time history from test 1 to 5

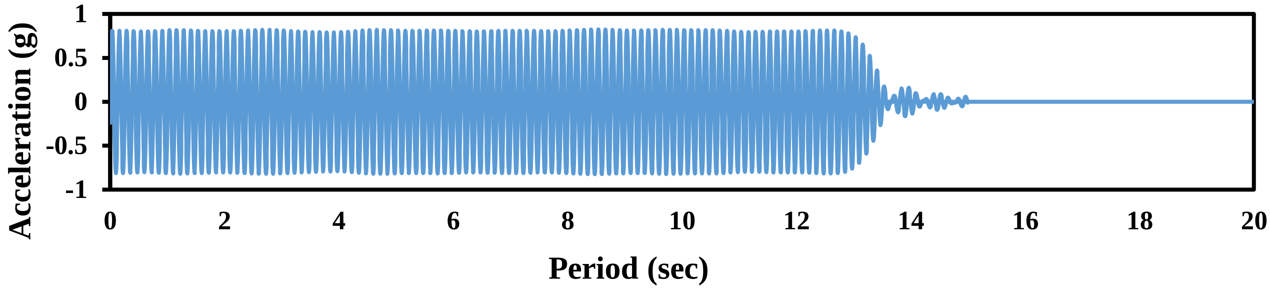

Fig. (b) Input acceleration time history of test 5

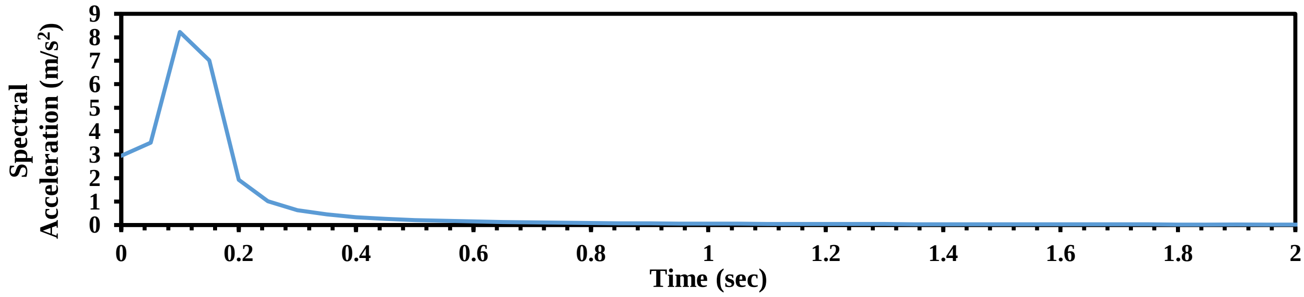

Fig. (c) Sa Spectrum for 5% damping (duration scaled) of test 5

3.4 Concrete specification

Preliminary concrete mix design has been calculated based on British Standard BS5328: Part 2: 1997. The calculated components of a concrete mix design for a quantity of $1m^3$ are shown in Table 4 (Franklin *et al.* 1988; Yip and Marsono 2016). A concrete mix design is prepared to achieve the concrete strength of 30MPa in 28days. In total, twenty-four cylindrical specimens for compressive and tensile strength of concrete are used. Each mould has a height of 200mm with a diameter of 100mm. Based on the laboratory tests, the average compressive and tensile strength of concrete is 33.26MPa and 12.86MPa, respectively.

In Fig. 7, the stress strain curve shows that the concrete starts to yield at strain 0.00069 with 26 N/mm^2 of stress. The concrete young's modulus test was stopped at compressive stress of 30.5 N/mm^2 due to the softening of cylindrical sample.

3.5 Instruments

The physical instruments and contact sensors that are attached at nine locations in the building frame structure during the test includes Accelerometer and Linear Variable Displacement Transformers LVDT are shown in Fig. 8. These instruments recorded the time histories of the building frame responses. Furthermore, the shaking table generates the seismic excitation based on input motion (frequency and displacement).

3.5.1 Accelerometers

In total, 7 accelerometers are attached to the framed specimen in which, three of them are attached to the shaking table to record the input 'g' values as suggested by EC8 (clause 3.2.3.1.2(4) and 3.2.3.1.3, page no. 43). The recorded data has a noise effect in each seismic motion signal. Authors studied the processing and adjustments in earthquake records (Chiu 1997; Boore and Bommer 2005; Boore 2001). To recover the correct data perfectly, Boore (2001) conducted a study and proposed correction methodologies to improve the actual shaking records. Boore and Bommer (2005) highlighted the effect of noise and proposed to perform baseline correction, where he recommended that a suitable cut off frequency was selected to filter out the data. Zero^{th} -order baseline correction was suggested in which a set of mean data recorded in pre-event would be removed from the entire data record in the very beginning stages of signal processing. The methodology supported to identify the changes in the velocity baseline followed by identification of a change in a particular instant of time and then subtracted the changes in baseline step of the acceleration data record. Then, the acceleration data baseline had been adjusted and corrected; it would easily integrate to get the numerical values of velocity and displacement. A study suggested that a time duration of 20 seconds and the methodology of baseline correction could not disturb the response spectrum of the recorded data set (Xian *et al.* 2017).

3.5.2 Linear Variable Displacement Transformers (LVDT)

A contact sensor LVDT is installed at four locations on a building frame that is shaking table base, building model base, intermediate story, and roof. In the shaking table, there is no fixed frame available to adjust the LVDT to record vertical displacement of the test framed specimen. Consequently, LVDT is placed to record the horizontal displacement at the joints of the beam and column at each story as shown in Fig. 8

3.5.3 Shaking table

A mega-torque motor was used to produce one dimensional shaking motion on a level platform (2m by 2m) by generating a mechanical torque repeatedly. The components of shaking table are shown in Fig. 9. The shaking table platform was lifted afloat by supplying an air pressure of 2 bars underneath the table platform to minimize the friction between the base and platform during cyclic horizontal movement. Vertical load of 2 to 4 tonnes can be placed on shaking table prior to shaking test. The shaking table was capable of producing frequencies of 0.1 – 20 Hz and horizontal displacements of 0.5-15 mm as shown in Fig. 10 (Lim *et al.* 2018).

For the horizontal shaking, performance of shaking table system is directly related to the input combinations of displacement and frequency as shown in Fig. 10. Moreover, Fig. 10 shows that the measured peak acceleration increased linearly with the input displacement at a particular frequency in shaking table (Lim *et al.* 2018). Thus, the highest peak acceleration that was achieved by using the shaking table system in the present study was about 0.82 gas shown in Table 6. This peak acceleration was achieved by inputting the frequency of 8 Hz and 0.5 unit of displacement.

3.6 Test procedure

This study considers a dynamic nonlinear vibration of an MDOF system with damping excluding the external applied forces. The Eq. (10) is used for the motion of the building model.

$$[M]\{\ddot{y}\} + [C]\{\dot{y}\} + [K]\{y\} = -[M]\{\ddot{x_g}\} \qquad (10)$$

Where [M] is the mass matrix, $\{y\}$ is the relative displacement vector, [C] is the damping matrix, [K] is the stiffness matrix and 'x_g' is the acceleration of ground motion. Furthermore, upper dot notation corresponds to time derivatives, i.e., $\{\dot{y}\}$ and $\{\ddot{y}\}$ correspond to velocity vector and acceleration vector, respectively.

Table 5 Seismic data of ground motion

Earthquake Event	Station	PGA 'g'(m/s^2)	Code name	Date and time
Mammoth Lake (ML)	Long Valley Dam (Upr L Abut)	0.34	ML1	25-05-1980, 4:34pm
		0.14	ML2	25-05-1980, 4:49pm
		0.33	ML3	25-05-1980, 7:44pm
		0.24	ML4	25-05-1980, 8:35pm

Table 6 Seismic input of artificial seismic sequence

Test case	Input motion		PGA 'g'(m/s^2)
	Frequency (Hz)	Displacement (mm)	
Test 1	3	1.5	0.25
Test 2	5	0.5	0.30
Test 3	3	2.0	0.36
Test 4	10	0.5	0.64
Test 5	8	0.5	0.82

3.6.1 Seismic Input

This study focuses on four real-time and five artificial earthquake motions. In the month of May and June 1980, approximately 1500 aftershock earthquakes were recorded at location Mammoth Lake, California (Archuleta *et al.* 1982). The series of real-time multiple seismic events occurred on 25th of May at Mammoth Lake (1980) has been extracted from the database of the Pacific Earthquake Engineering Research Center (PEER, 2019) as listed in Table 5.

Regarding the artificial ground motion, in UTAR, Malaysia, shaking table performed harmonic motions which were able to simulate 0.82 'g' maximum value and considering uniform patterns of the signal. Furthermore, shaking table motion was unidirectional moving along the Y-axis as shown in Fig. 3. Shaking table requires combination of two input parameters that is frequency and displacement. Therefore, before performing the test on frame specimen, various seismic excitations are determined through these input motions. Afterward, the building model is subjected to five different artificial harmonic ground motions used sequentially ranging from 0.25g to 0.82g.

Furthermore, the time duration is 15 seconds for all five seismic ground motions. The input ground motions recorded from accelerometer are shown in Table 6.

The PGA values are utilized in increasing order as shown in Fig. 11(a). It is observed that in Fig. 11 (a), each ground motion (that is Test 1, 2, 3, 4 and 5) has a uniform harmonic wave. Moreover, the acceleration time history and spectrum of ground motion for Test 5, with maximum acceleration is shown in Fig. 11 (b) and (c).

3.7 Signal processing and analysis

The measured acceleration data are processed by removing the baseline drift and unwanted noises from the actual signal before they are used for subsequent analysis. Simple quadratic baseline correction and Butterworth low

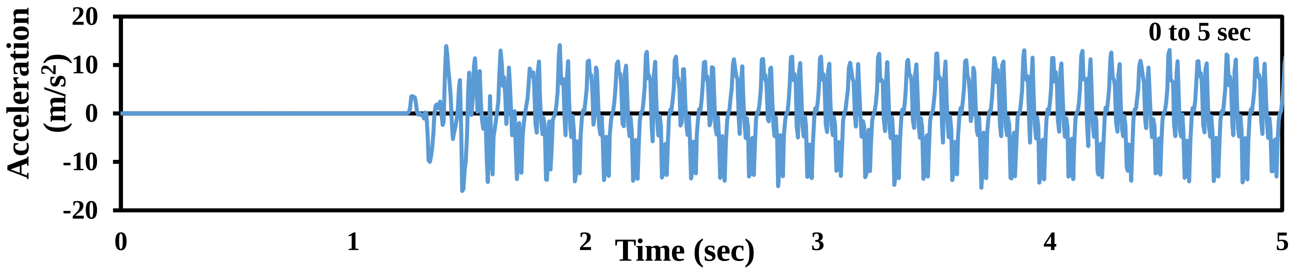

Fig. 12 (a) Recorded Acceleration time series under input frequencies at Test 4 (10 Hz)

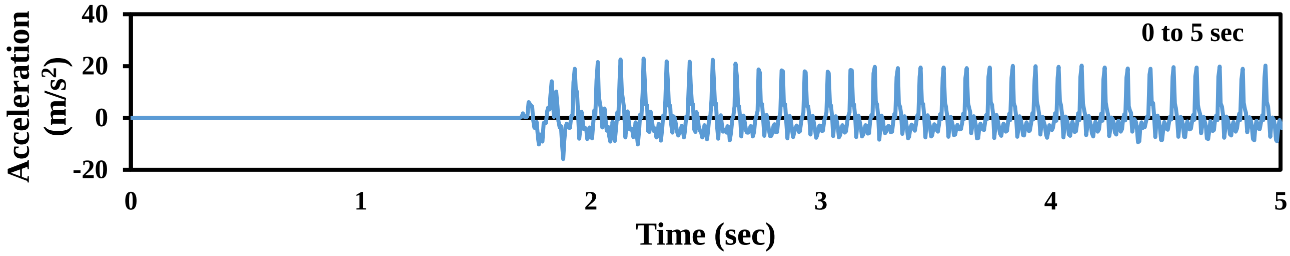

Fig. 12 (b) Recorded Acceleration time series under input frequencies at Test 5 (8Hz)

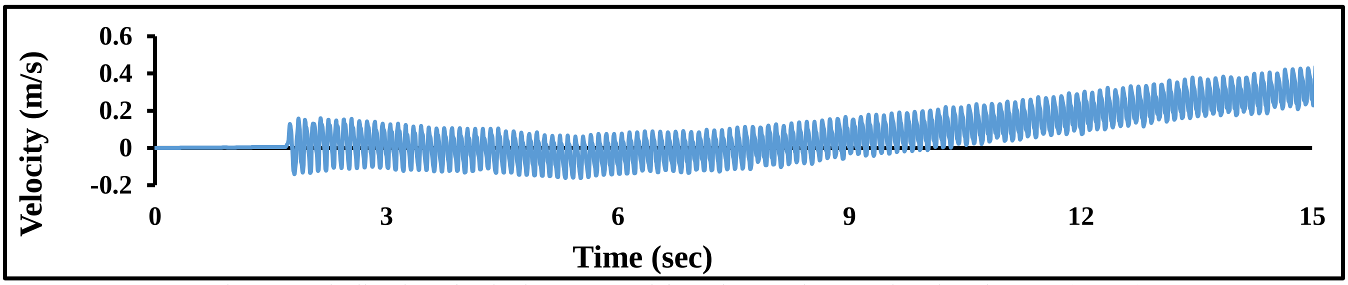

Fig. 13 Periodic plot of velocity extracted from integrating acceleration data set (Test 4)

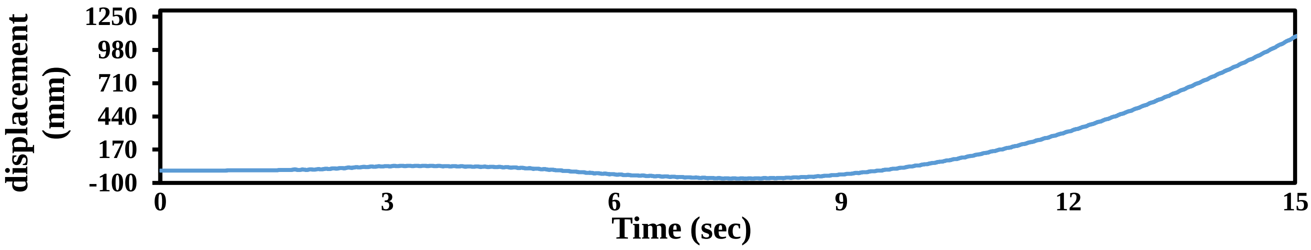

Fig. 14 Plot of displacement time series through integrating the acceleration data (Test 4)

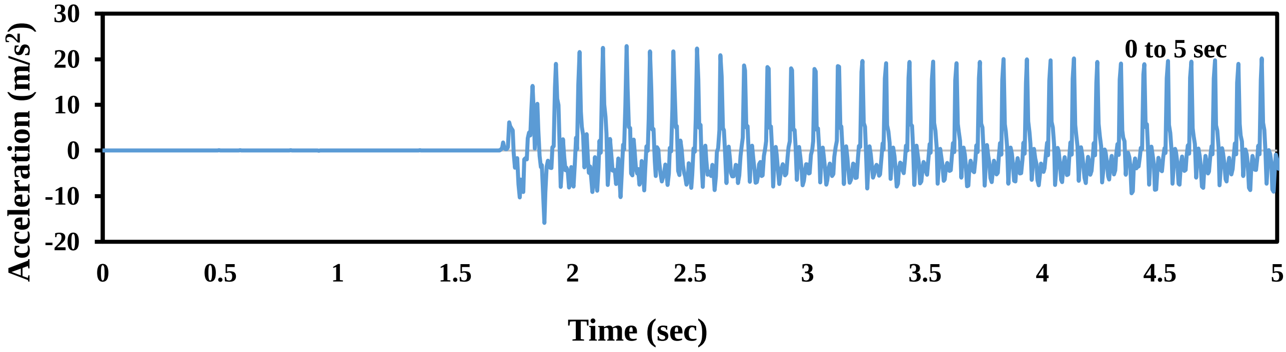

Fig. 155 Acceleration data from accelerometer after baseline correction (Test 4)

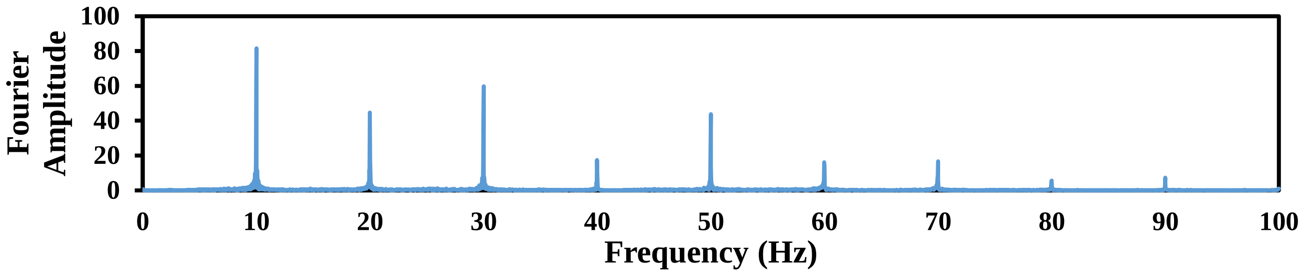

Fig. 16 Fourier Amplitude after Baseline Correction (Test 4)

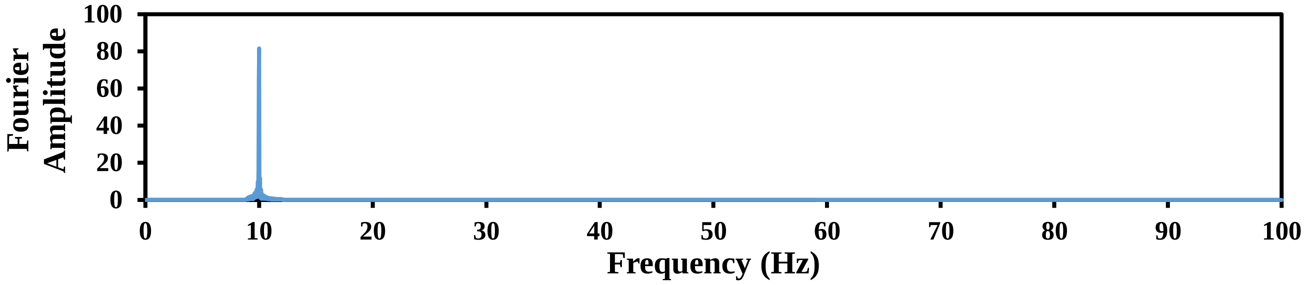

Fig. 177 Fourier Amplitude after Butterworth low pass filtering (Test 4)

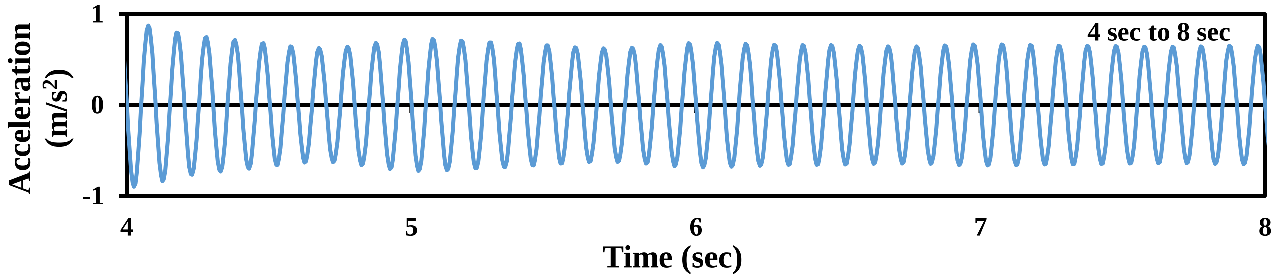

Fig. 188 Acceleration data from accelerometer after Butterworth low pass filtering (Test 4)

pass (high-cut) filtering methods are attempted to process the raw acceleration data. After that this data was matched with data achieved by simulation software ETABS which tends to show the real behavior between the test framed specimen and simulated model.

In Test 4 and 5, the input frequency is 10Hz and 8Hz respectively. The raw data as recorded by the accelerometer as shown in Fig. 12 indicates a noise. Therefore, it was required to use a suitable signal processing methodology to remove unwanted data, associated with the measured acceleration data. Acceleration data in Fig. 12 was integrated to get velocity and displacement with respect to periodic time series. The integration method to obtain numerical data set in this study was taken from Berg and Housner (1961). The time series of velocity and displacement as shown in Fig. 13 and Fig. 14 was found to have a shift in the baseline. In the displacement plot, the wave moves toward the (-) X axis referring to negative direct current bias in the acceleration plot recorded by an accelerometer.

Fig. 14 shows that the maximum displacement recorded at the end of the displacement time series plot is 1100mm which is much higher than actual and input value. The wavy nature in displacement time series plot and shifting of baseline, occurred due to rotational motion (Graizer 2006) of a building model and presence of low-frequency noises. Baseline correction has a tendency to eliminate the lower frequencies and considers the higher frequency which is, in fact, a high pass filtering method with an unidentified cut off frequency (Boore and Bommer 2005). Thus, the maximum displacement time series data is required to be corrected otherwise the end results will be unexpected and inappropriate.

The original data recorded by the accelerometer is first introduced to correction methodology known as Simple quadratic baseline correction by using the Seismosignal software which is based on Eqs. (11-13) (Technical information sheet 2018). This correction scheme subtracted the entire acceleration data from a quadratic least-square fitting line prior to numerical integration.

$$\text{Acceleration} \quad = \quad a_t - (a_0 + a_1 t) \tag{11}$$

$$\text{Velocity} \quad = \quad v_t - \left(a_0 t + \tfrac{1}{2}\, a_1 t^2 \right) \tag{12}$$

$$\text{Displacement} \quad = \quad D_t - \left(\tfrac{1}{2}\, a_0 t^2 + \tfrac{1}{6}\, a_1 t^3 \right) \tag{13}$$

Where, a_t is acceleration (m/s^2), v_t = velocity (m/s), D_t = displacement (mm), t = time (sec) and a_0, a_1 = coefficients.

In Fig. 155, the problem of baseline drift is resolved however the data corrected by a Simple quadratic baseline

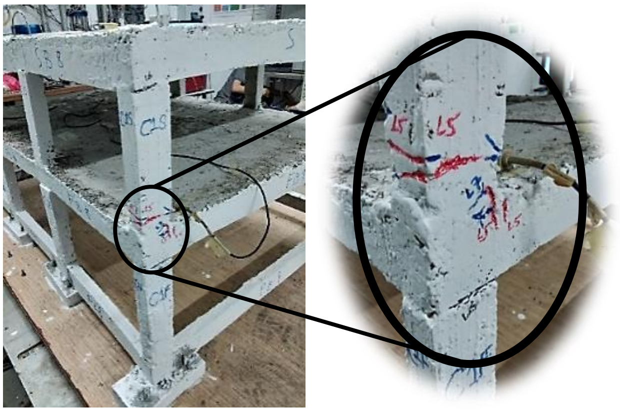

Fig. 19 (a) flexural horizontal minor cracks at the column in storey 1

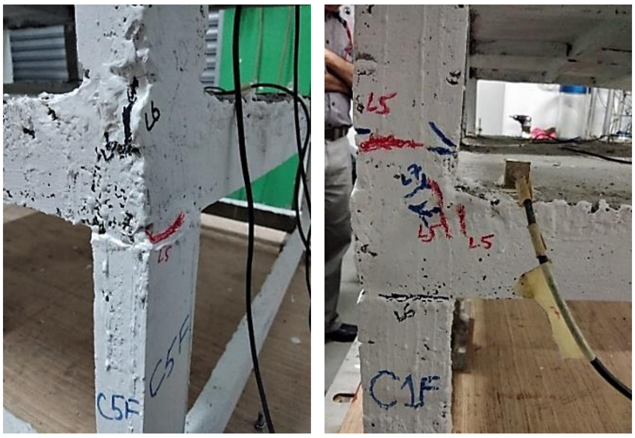

Fig. 19 (b) Flexural horizontal and vertical cracks at a beam-column joint in storey 1

still shows the noise in the waveform because baseline correction is effective in eliminating long-period or low-frequency noise, however, it lacks in removing high-frequency noises.

In Fig. 16, the shaking frequency is set to 10 Hz for Test 4 however, frequencies of higher than 10 Hz are still observed. Fourier amplitude spectrum in Fig. 16 shows that there is a need to remove the unwanted frequencies in the signal. Low-pass filtering technique is proposed by selecting a realistic cut-off frequency (Boore and Bommer 2005) for this study.

Therefore, Butterworth's low-pass (high-cut) filtering technique is used to remove the higher-frequency noise (Boore and Bommer 2005) as shown in Fig. 17 and Fig. 18. Thus, the Butterworth low pass filtering method is adopted as the signal processing method in the present study as the acceleration profile obtained upon performing the filtering method shows the best agreement.

4. Experimental and simulated test results

The results presented in this section includes the dynamic behavior of the experimental and simulated framed model. The section focuses on the observed response of the framed structure, maximum displacement, residual displacement, interstorey drift ratio, and damage limitation. Moreover, the building model has passed through multiple sequential seismic excitations (artificial and real-time ground motion). Therefore, the structural behavior in all the seismic ground motions have been discussed in this section.

4.1 Observed response and cracks pattern

In the framed specimen Test 1 and 2, shaking of the building model is observed however there are no cracks formed. Particularly intermediate beams and columns has no effect of artificial ground motions. In Test 3, the test model shows the damage behavior. The horizontal, vertical and diagonal cracks are observed at the beam-column joint as well as corner at storey 1 as shown in Fig. 19 (a) and (b). The cracks are formed due to transfer of moments from beam end to column ends. This damage points to the yielding of the beam and column reinforcement.

Moreover, the model is observed with significant horizontal cracks in the beam-column joint of the roof (storey 2) as shown in Fig. 20. Intermediate columns and beams have not shown any significant damage behavior during this artificial ground motion.

During the Test 4 run, the model has experienced significant cracks at beam-column joint at the base and storey 1 as shown in Fig. 21 (a) and (b) which is the extension of cracks propagated in Test 3. At this artificial ground motion, intermediate columns and beams of the framed specimen experience cracks as shown in Fig. 21 (c) and (d). However, there is no spalling of concrete observed.

Lastly, Test 5 has maximum PGA of 0.82g which caused the higher frequency of vibration however the test specimen sustains and absorb vibrations without any member failure. This seismic sequence further propagates the cracks at inner joints of column and beam as presented in Fig. 22.

Therefore, under successive incremental seismic ground motion, concrete material deterioration starts from storey 1 to the adjacent storey due to the impact of inertial forces in the horizontal direction. The damage concentration in the framed structure is observed to be at the beam-column joints. The damage is less severe especially at the storey 2 as compared to the other story. No structural failure is recorded other than concrete cracks and reinforcement internal plasticity. Thus, it is established that the building model with ductility class low (DCL) has a tendency to absorb lower to higher 'g' values and resist the earthquake loading due to the strength of framed structure rather than its ductility.

4.2 Maximum displacement response

Fig. 23 shows the time histories of maximum displacement of storey 1 and 2 for sequential ground motions from test 1 to test 5. Moreover, shaking table results are found to be near to the simulated model results from ETABS. The test framed specimen indicates that the building model has a progressive permanent displacement which tends to increase the maximum displacement of each oncoming successive seismic ground motions. In each Test from 1 to 5, uniform harmonic displacement has been observed simultaneously. Fig. 23 represents that test 3(0.34g) has displaced model 63.7mm and 91.0mm in in storey 1and 2 as compared with test 5 (0.82g) having displacements of 44.5mm and 75.9mm in storey 1 and 2. Additionally, in test 2, storey 1 and 2 maximum displacements are approximately three-fold then test 1.

Fig. 20 Flexural horizontal cracks at roof beam column joint

Fig. 21 (a)

Fig. 21 (b)

Fig. 21 Significant cracks at (a) base; (b) storey 1

Fig. 21 (c)

Fig. 21 (d)

Fig. 21 Significant cracks at (c) intermediate column and (d) beam-column joint

Fig. 22 (a)

Fig. 22 (b)

Fig. 22 (c)

Fig. 22 (d)

Fig. 22 (a) Severe flexural crack at periphery beam at base; (b) significant flexural crack at periphery beam at storey 1 (c) flexural crack in the internal beam-beam joint at storey 1; (d) flexural cracks in beam-column joint at storey 2 slab

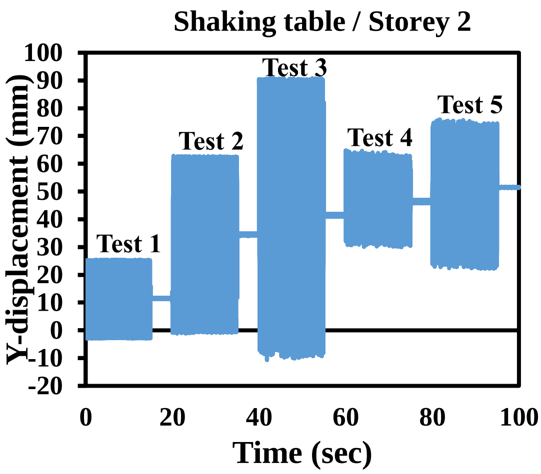

Fig. 23 (a)

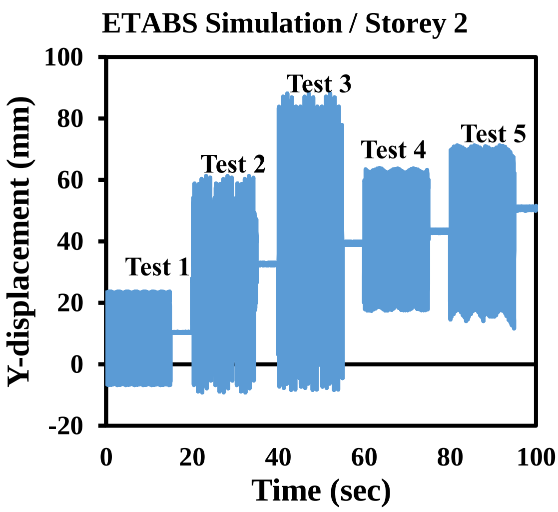

Fig. 23 (b)

Fig. 23 (a) and (b) Time history of Y-axis horizontal displacement under artificial seismic sequence

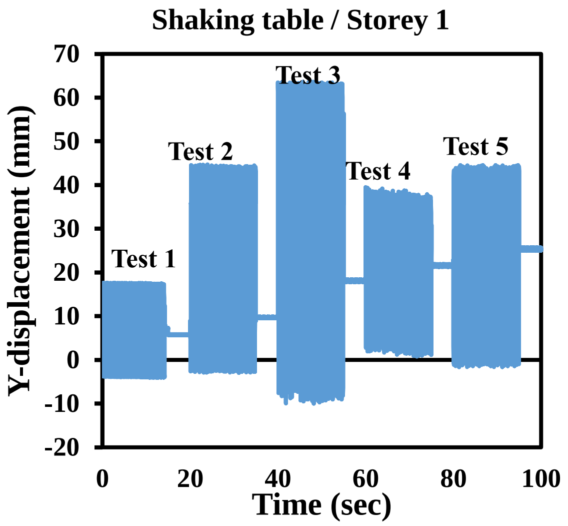

Fig. 23 (c)

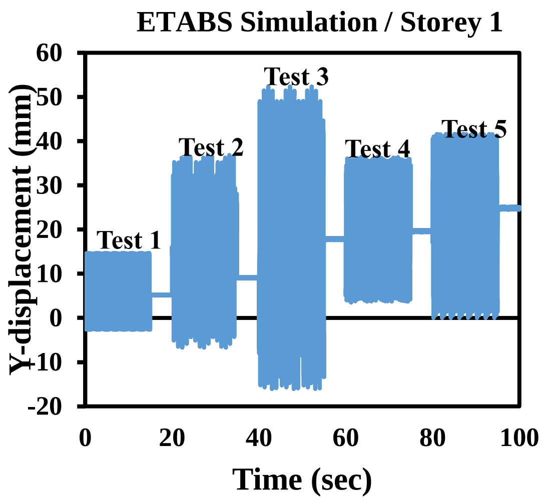

Fig. 23 (d)

Fig. 23 (c) and (d) Time history of Y-axis horizontal displacement under artificial seismic sequence

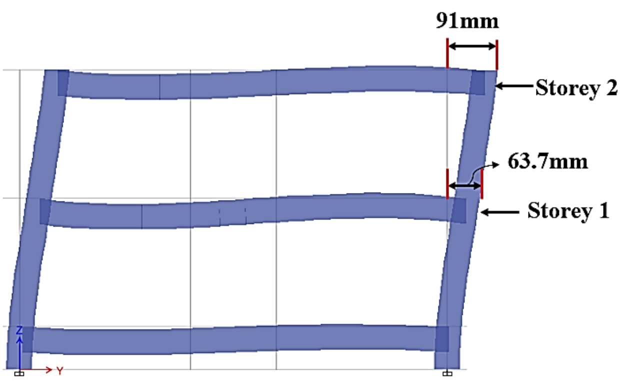

Fig. 24 Highest displacement image in Test 3

Here, Fig. 23 illustrates that model highest displacement of the model recorded in Test 3. Moreover, Fig. 24 shows the maximum displacement attained by model in the sequential ground motion. A two dimensional image in Fig.

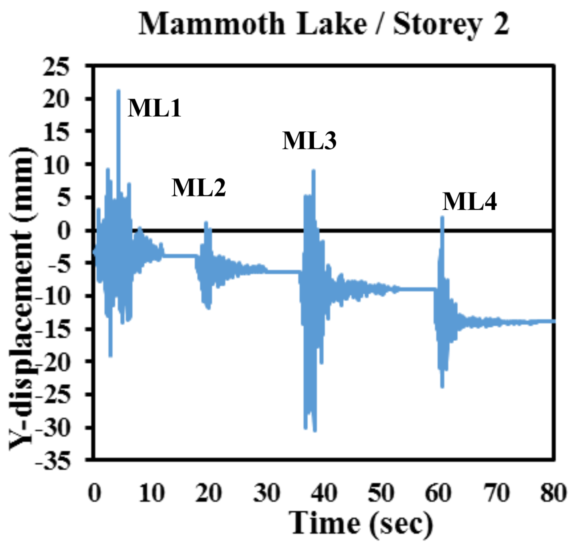

Fig. 25 (a)

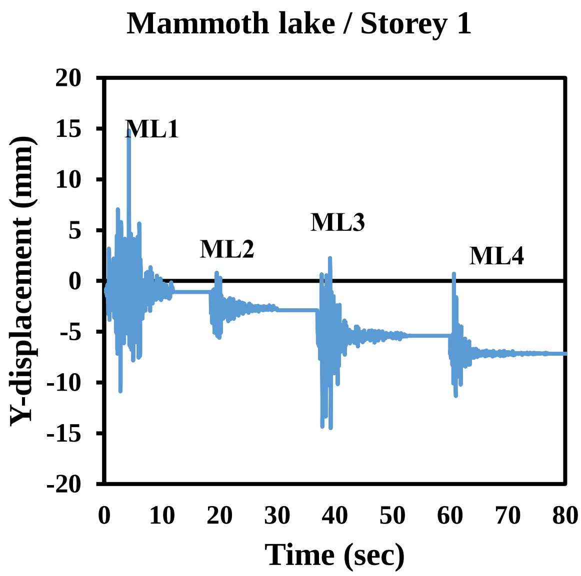

Fig. 25 (b)

Fig. 25 (a) and (b) Horizontal displacement time histories at storey 1 and 2

24 show the maximum displacement in storey 1 and 2 was found to be 63.7mm and 91mm, respectively.

To further asses the building model, the framed specimen has been examined on real seismic ground motions as shown in Fig. 25. The sequential excitations show the behavior of building model in a different manner. The PGA of ML1 and ML3 are similar that is 0.34g and 0.33g however, the model displaces maximum 30.4mm in ML3 representing the permanent displacement in the model. Additionally, surface acceleration and magnitude of an earthquake affects the maximum displacement. Therefore, building model may excite in a different mode in each sequential seismic ground motions. Thus, it can be summarized that results can vary based on the characteristics of framed specimen and successive ground motions.

4.3 Maximum residual displacement

The sequential ground motion had strongly affected the test specimen and increases the residual displacement in each successive excitation. Fig. 26 shows that the residual displacement in storey 2 is more than the storey 1 in each sequential earthquake motions. Fig. 26 (a) and (b) had similar effects of displacement which satisfy the results of shaking table and ETABS simulation outcomes. In successive ground motions, it was observed that the residual displacement accumulated with respect to incremental PGAs'. Most importantly, it has been observed that experimental model does not show any cracks in Test 1 (0.25g) and Test 2 (0.30g) as mentioned earlier however it can clearly be seen in Fig. 26 (a) that Test 1 and 2 have residual displacements of 5.76mm and 9.70mm in storey 1, similarly 11.53mm and 34.57mm in storey 2 which clearly highlights the reinforcement internal plasticity during the shaking table test.

Fig. 26 (c) showed that ML1 presents the least residual displacement that is 1.08mm and 4.0mm at storey 1 and 2 respectively. In ML4, the sequential excitations accumulate the displacement threefold in storey 2 and sevenfold in storey 1 respectively. Thus, it is evident that the first seismic motion affects the stiffness and degrade the strength of the building model which causes the framed structure to displace permanently.

4.4 Interstorey drift ratio and verification of damage limitation

Interstorey drift ratio (IDR) is one of the most critical parameters in structural analysis and design. It is the maximum relative displacement between two consecutive stories divided by the storey height. Interstorey drift ratio (IDR) also helps to check the structural damage limitations with respect to EC8. Fig. 27 (a) and (b) show the maximum interstorey drift ratio followed by sequential ground motions from Test 1 to Test 5. In storey 1, it is evident that damage limitation of test 3 (simulated and experimental outcomes) reached maximum drift 1.56% and 1.84% in successive seismic motions. In both stories, the figure clearly shows that succeeding seismic vibration after the very first ground motion lead to higher drift. Additionally, Torey 1 has maximum IDR as compared with storey 2 which represented the behavior of building model under strong repeated seismic motions. Furthermore, Fig. 27 (a) shows that the building model placed on shaking table has crossed damage limitation 1% even though there is no structural damage being recorded as shown in Figs. 19-22 which clearly shows that EC8 undermined the damage limit criteria under sequential ground motions.

Fig. 27 (c) show that the real-time sequential seismic vibrations do not illustrate any significant drift effect due to lower PGAs', however, the building model excites in different modes in oncoming real-time seismic sequence. Thus, the findings clearly show that successive seismic vibration increase IDR depending on its ground accelerations.

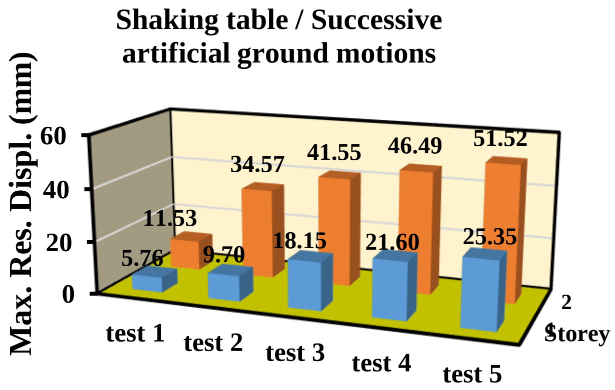

Fig. 26 (a)

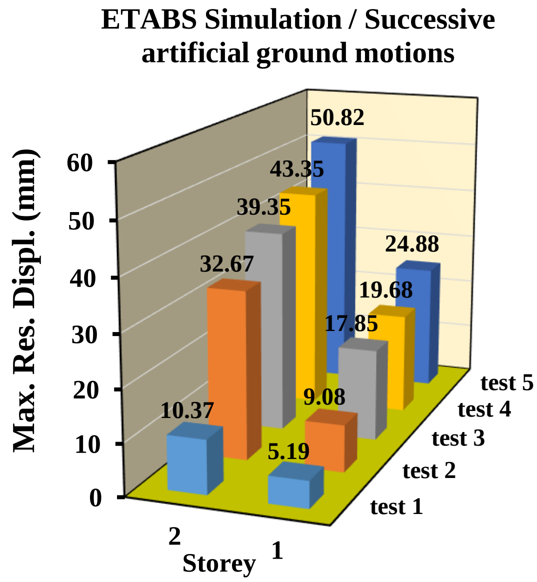

Fig. 26 (b)

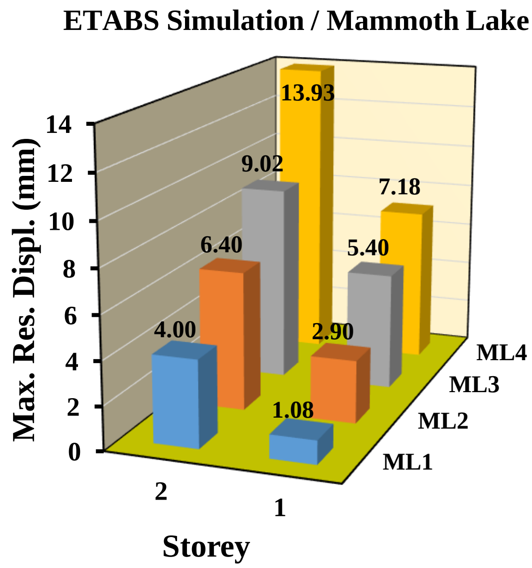

Fig. 26 (c)

Fig. 26 (a), (b) and (c) Maximum Residual Displacement under sequential ground motions

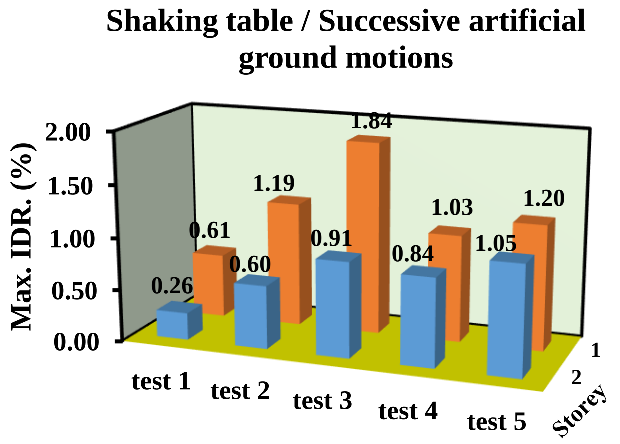

Fig. 27 (a)

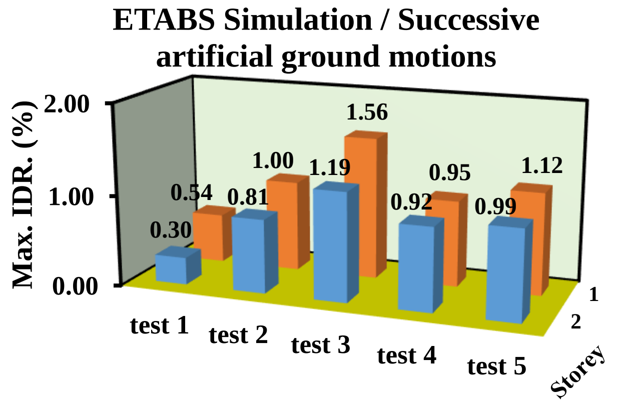

Fig. 27 (b)

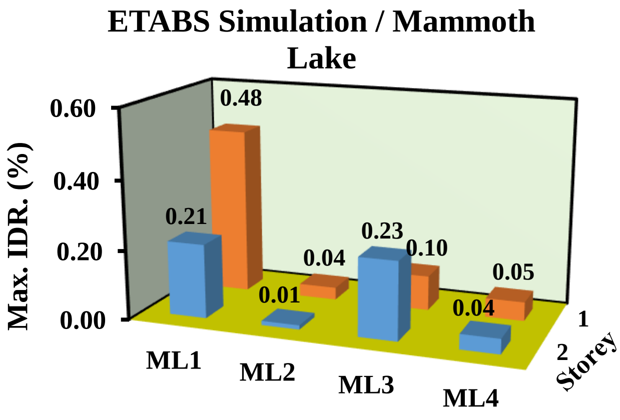

Fig. 27 (c)

Fig. 27 (a), (b) and (c) Maximum Interstorey Drift Ratio under sequential ground motions

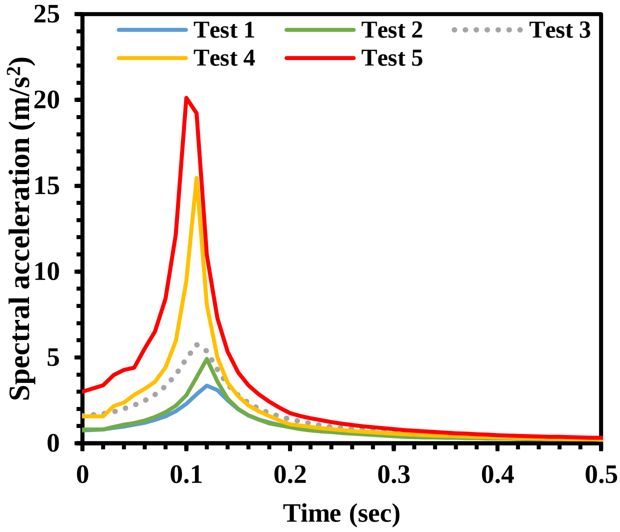

Fig. 28 Response spectrum graphs and natural period of vibration under artificial ground motions

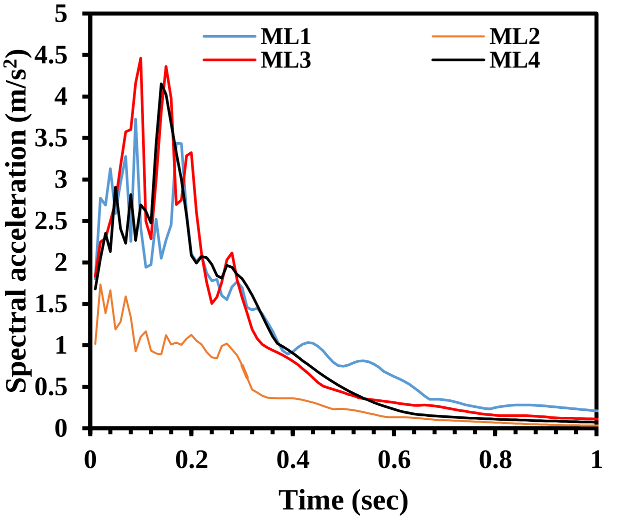

Fig. 29 Response spectrum graphs and natural period of vibration under real ground motions

4.5 Spectral acceleration and Fourier spectrum

Spectral acceleration defines the maximum acceleration experienced by the building model due to the ground acceleration. Fig. 28 shows the response spectrum graph of the experimental model at storey 2 under artificial ground motions. In Test 1, maximum acceleration is 3.4m/s^2 at natural period of vibration 0.12sec as shown in Fig. 28. Moreover, acceleration of 4.9m/s^2 and 5.7m/s^2 is observed at 0.12sec and 0.11sec in Test 2 and Test 3, respectively. It is noteworthy to highlight that, as the ground acceleration increases from Test 1 to Test 3, spectral acceleration in storey 2 increases and natural periodic vibration decreases. Lastly, in Test 4 and 5, observed spectral accelerations are 15.4m/s^2 and 20.12m/s^2 at 0.11sec and 0.10sec, respectively.

In real ground motions, Fig. 29 shows that the spectral acceleration 3.73m/s^2 has been observed at 0.11sec in ML1. Moreover, the maximum acceleration recorded in storey 2 is 4.46m/s^2 at 0.10sec in ML3. It is noteworthy to highlight that PGAs' of ML1 and ML3 are similar i.e. 0.34g and 0.33g, however, under sequential ground motions, the natural period of vibration reduces from ML1 to ML3. Additionally, the maximum acceleration (i.e. 4.46m/s^2) in ML3 under real ground motions could not even cross the incremental acceleration (i.e. 4.9m/s^2) observed in Test 2

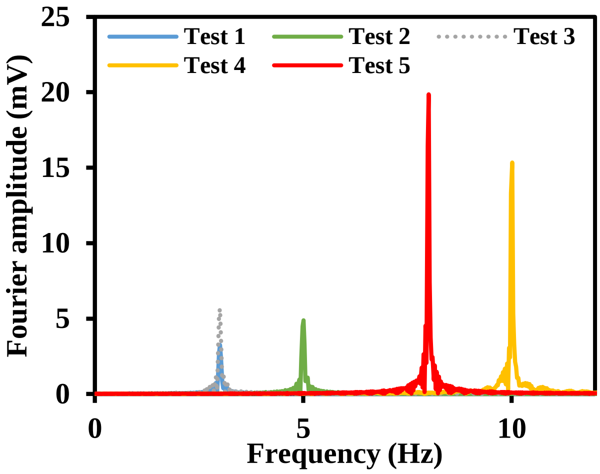

Fig. 30 Fourier spectrum under artificial ground motions

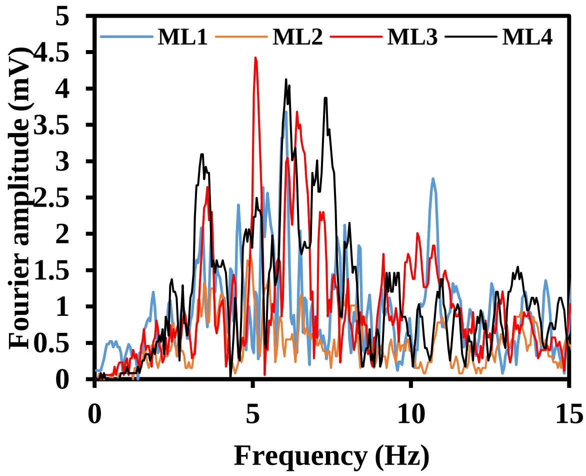

Fig. 31 Fourier spectrum under real ground motions

under artificial ground motion, which shows the intensity of harmonic waves in artificial produced ground motions. Thus, response spectrum graphs in Fig. 28 and Fig. 29 clearly illustrate that the building model experiences incremental spectral accelerations under sequential ground motions, which causes dwindling in natural periodic vibration.

Fig. 30 shows the Fourier spectrum of artificial ground motions. It can clearly be observed that the dominant frequency in the sequential motions is 8Hz in Test 5. The minimum and maximum amplitude found in Fig. 30 are 3.32mV (Test 1) and 19.86mV (Test 5), respectively. Moreover, the input frequency in Test 1 and Test 3 are same (i.e. 3Hz), however, it is witnessed that Test 3 has higher amplitude (5.69mV) as compared to Test 1 (3.32mV). In real ground motions, Fig. 31 shows the Fourier spectrum of the seismic waves. Each real ground motion i.e. ML1, ML2, ML3 and ML4 have a dominant frequency such as 6.05Hz, 4.93Hz, 5.07Hz, and 6.05Hz, respectively. However, the maximum amplitude witnessed in sequential motion is 4.43mV in ML3, which is less than the amplitude 4.86mV observed in Test 2. Thus, it is concluded that the model has the ability to resist real and intense artificial ground motions.

5. Conclusions

To predict the behavior of a building model for sequential ground motion from low to high, Peak Ground Acceleration (PGA) values, a shaking table test had been performed to gather the data of low-rise RC framed building model. Moreover, ETABS simulation had been run to validate the results with shaking table outcome. Additionally, the framed structure also analyzed with a real-time seismic sequential motion with the help of simulated software ETABS. This study produced a standard assessment database which could be used for verification of results stating the effects of sequential seismic ground motions on RC framed structures. The following observations and conclusions are made for artificial and real ground motions:

- In artificial ground motions, different response, characteristic and configurations after each seismic sequence have been observed. In the shaking table test, structural damage is witnessed due to incremental sequential ground motions ranging between 0.25g to 0.82g. Moreover, it is found that few structural members of the building model behave inelastically during successive ground motions. Additionally, the framed model highlights the structural strength against its ductility.
- The horizontal displacement for storey 1 and 2 increase with corresponding to artificial successive ground motion. Each storey displaces twofold in Test 2 as compared with Test 1. In Test 3 (0.36g), building model displaces maximum 63.7mm and 91.0mm at storey 1 and 2 in correlation with maximum displacement of 44.5mm and 75.9mm in storey 1 and 2 at Test 5 (0.82g) which indicates that Test 3 has the maximum seismic effect on the framed structure in all the five sequential seismic motions.
- Residual displacement increases in result of sequential ground motions because the first seismic motion affects the stiffness of the building model and cause the structure to displace permanently. Moreover, in experimental model, Test 1 and 2 have residual displacements of 5.76mm and 9.70mm in storey 1, similarly 11.53mm and 34.57mm in storey 2 which shows the reinforcement internal plasticity during the shaking table test.
- The framed model shows maximum IDR in storey 1 as compared to storey 2 and increases IDR with respect to successive artificial ground motions. Additionally, in storey 1, damage limitation of test 3 (simulated and experimental outcomes) reached maximum drift 1.56% and 1.84% in successive seismic motions which clearly shows that EC8 underestimated the damage criteria for seismic ground motions.
- In real ground motions, ML3 reached to 30.4mm maximum displacement i.e. 57% higher than ML1, however, it is noteworthy that ML1 and ML3 PGAs' were similar. Additionally, maximum displacement recorded in ML3 in real ground motions could not cross the displacement 62.8mm recorded in Test 2 in artificial ground motions, which shows that model performed well in real ground motions and faced the intense ground vibrations in artificial seismic waves.

- In residual displacement, it is obvious that the first real ground motion disturbs the stiffness and reduce the strength of the building model which makes the model to displace permanently, however, still, model reached to 13.93mm displacement (ML4), which only crosses the permanent displacement 11.53mm (Test 1) of artificial ground motions.

Acknowledgments

The authors acknowledge the financial support through UTAR-RF grant no. IPSR/RMC/UTARRF/2016-C1/Z1 provided by Universiti Tunku Abdul Rahman (UTAR), Perak, Malaysia.

References

Abas, M.R.C. (2001), "Earthquake Monitoring in Malaysia", *Seismic Risk Seminar, Malaysia*, Seismological Division, Malaysian Meteorological Service.

Abas, M.R.C., Musa, R.C., Ahmad, Z., Rahim, I.A., Tongkul, F., Bakar, R.A., Surip, N., Manap, M.A., Jamaludin, T.A. and Shuib, M.K. (2017), "Active Faults in Peninsular Malaysia with Emphasis on Active Geomorphic Features Of Bukit Tinggi Region", *Malaysian J. Geosci.*, **1** (1), 13–26. https://doi.org/10.26480/mjg.01.2017.13.26.

Adiyanto, M.I., and Majid, T.A. (2014), "Seismic design of two storey reinforced concrete building in Malaysia with low class ductility", *J. Eng. Sci. Technol.*, **9**(1), 27–46.

Akadiri, P.O., Chinyio, E.A., and Olomolaiye, P.O. (2012), "Design of a sustainable building: a conceptual framework for implementing sustainability in the building sector", *Buildings*, **2**(2): 126–52. https://doi.org/10.3390/buildings2020126.

Amadio, C., Fragiacomo, M., and Rajgelj, S. (2003), "The effects of repeated earthquake ground motions on the non-linear response of SDOF systems", *Earthq. Eng. Struct. Dynam.*, **32**(2), 291–308. https://doi.org/10.1002/eqe.225.

Archuleta, R.J., Cranswick, E., Mueller, C., and Spudich, P. (1982), "Source parameters of the 1980 Mammoth Lakes, California, Earthquake sequence", *J. Geophys. Res.*, **87**(B6), 4595–4607. https://doi.org/10.1029/JB087iB06p04595.

Bahadir, F., and Balik, F.S. (2018), "Behaviour of 3D RC frames placed at different angles on shaking table", *J. Croatian Assoc. Civil Eng.*, **70**(3), 171–186. https://doi.org/10.14256/jce.1655.2016.

Berg, G.V., and Housner, G. W. (1961), "Integrated velocity and displacement of strong earthquake ground motion", *Bullet. Seismologic. Soc. America*, **51**(2), 175–189.

Boore, D.M. (2001), "Effect of baseline corrections on displacements and response spectra for several recordings of the 1999 Chi-Chi, Taiwan, Earthquake", *Bullet. Seismologic. Soc. America*, **91**(5), 1199–1211.

Boore, D.M., and Bommer, J.J. (2005), "Processing of strong-motion accelerograms: Needs, Options and Consequences", *Soil Dynam Earthq. Eng.*, **25**, 93–115. https://doi.org/10.1016/j.soildyn.2004.10.007.

Chiu, H.C. (1997), "Stable baseline correction of digital strong-motion data", *Bullet. Seismologic. Soc. America*, **87**(4), 932–44.

Eurocode 2 (2004), Design of concrete structures. Part 1.1: General rules and rules for buildings Eurocode, European Committee for Standardization; Brussels, Belgium.

Eurocode 8 (2004), Design of structures for earthquake resistance. Part 1: General rules, seismic actions and rules for buildings, European Committee for Standardization; Brussels, Belgium.

Faisal, A., Majid, T.A., and Hatzigeorgiou, G.D. (2013), "Investigation of story ductility demands of inelastic concrete frames subjected to repeated earthquakes", *Soil Dynam Earthq. Eng.*, **44**, 42–53. https://doi.org/10.1016/j.soildyn.2012.08.012.

FEMA368 (2000), NEHRP recommended provisions for seismic regualtions for new buildings and other structures, Federal Emergency Management Agency; Washington D.C., USA.

Franklin, R.E., Erntroy, H.C. and Marsh, B.K. (1988), *Design of Normal Concrete Mixes*, 2nd Edition, Technology and Engineering, USA.

Graizer, V. (2006), "Tilts in strong ground motion", *Bullet. Seismologic. Soc. America*, **96**(6), 2090-2102. https://doi.org/10.1785/0120060065.

Hatzivassiliou, M., and Hatzigeorgiou, G.D. (2015), "Seismic sequence effects on three-dimensional reinforced concrete buildings", *Soil Dynam Earthq. Eng.*, **72**, 77–88. https://doi.org/10.1016/j.soildyn.2015.02.005.

Heuisoo, H., Mincheol, P., Sangki, P., Juhyong, K., and Yong, B. (2019), "Experimental verification of methods for converting acceleration data in high-rise buildings into displacement data by shaking table test", *Appl. Sci.* **9**(8), 1653. https://doi.org/10.3390/app9081653.

Hosseinpour, F., and Abdelnaby, A.E. (2017), "Effect of different aspects of multiple earthquakes on the nonlinear behavior of RC structures", *Soil Dynam Earthq. Eng.*, **92**, 706–725. https://doi.org/10.1016/j.soildyn.2016.11.006.

Ismail, R., Ibrahim, A., and Adnan, A. (2018), "Damage assessment of medium-rise reinforced concrete buildings in Peninsular Malaysia subjected to Ranau Earthquake", *J. Civil Eng. Technol.*, **9**(7), 881–888. https://uitm.pure.elsevier.com/en/publications/damage-assessment-of-medium-rise-reinforced-concrete-buildings-in.

Ismail, R., Ibrahim, A., and Adnan, A. (2016), "Seismic damage analysis of reinforced concrete frame of public buildings in Ipoh subjected to Acheh Earthquake event", *InCIEC 2015*, 149–157. https://link.springer.com/chapter/10.1007/978-981-10-0155-0_15.

Ismail, R., Ibrahim, A., and Adnan, A. (2016), "Vulnerability of high-rise buildings in Kuala Lumpur subjected to Acheh earthquake event", *InCIEC 2015*, 139–147. https://link.springer.com/chapter/10.1007/978-981-10-0155-0_14.

Ismail, R., Ibrahim, A., and Norhazlila, R. (2017), "Vulnerability study of public buildings subjected to earthquake event", *MATEC Web of Conferences*, **103**(02023). https://doi.org/https://doi.org/10.1051/matecconf/201710302023.

Ismail, R., and Zamahidi, N.F. (2015), "An evaluation of high-rise concrete building performance under low intensity earthquake effects", *InCIEC 2014*, 79–86. https://link.springer.com/chapter/10.1007%2F978-981-287-290-6_7.

Ismail, R. (2018), "Seismic performance for vertical geometric irregularity frame structures", *IOP Conference Series: Earth and Environmental Science*, **140**(1). https://doi.org/https://doi.org/10.1088/1755-1315/140/1/012101.

Ismail, R., Hamidah, M.S., and Hassim, M. (2014), "Evaluation of medium-rise reinforced concrete building performance under low intensity earthquake effect", *Appl. Mech. Mater.*, **661**, 106–110. https://doi.org/https://doi.org/10.4028/www.scientific.net/AMM.661.106.

Khoshraftar, A., Abbasnia, R. and Raof, F.F. (2013), "The effect of degradation on seismic damage of RC buildings", *Adv. Environ. Biology*, **7**(5), 861–867.

Lim, J.X., Lee, M.L., and Tanaka, Y. (2018), "1g shaking table tests on residual soils in Malaysia through different model setups", *Geomech. Eng.*, **16**(5), 547-558

Manafpour, A., and Moghaddam, P.M. (2019), "Performance capacity of damaged RC SDOF systems under multiple far and near-field earthquakes", *Soil Dynam Earthq. Eng.*, **116**, 164–173. https://doi.org/10.1016/j.soildyn.2018.09.045.

Marto, A., and Kasim, F. (2013), "Seismic impact in Peninsular Malaysia", *The 5th International Geotechnical Symposium-Incheon*, 237–242. https://doi.org/10.13140/2.1.3094.9129.

Megawati, K., Lam, N.T.K., Chandler, A.M., and Pan, T.C. (2004), "Cities without a seismic code I : hazard assessment", *13th World Conference on Earthquake Engineering*, 129-145.

Moehle, J., and Deierlein, G.G. (2004), "A framework methodology for performance-based earthquake engineering", *13Th World Conference on Earthquake Engineering*, 679-692.

Moustafa, A., and Takewaki, I. (2011), "Response of nonlinear single-degree-of-freedom structures to random acceleration sequences", *Eng. Struct.*, **33**(4), 1251–1258. https://doi.org/10.1016/j.engstruct.2011.01.002.

MS EN 1998-1 (2015), Design of structures for earthquake resistance. Part 1: General Rules, Seismic Actions and Rules for Buildings, Department of Standards Malaysia, Selangor, Malaysia.

Oyguc, R., Toros, C. and Abdelnaby, A.E. (2018), "Seismic behavior of irregular reinforced-concrete structures under multiple earthquake excitations", *Soil Dynam Earthq. Eng.*, **104**, 15–32. https://doi.org/10.1016/j.soildyn.2017.10.002.

PEER (2019), Strong motion data base; Pacific Earthquake Engineering Research Center, Berkeley, USA. http:www.peer.berkeley.edu/smcat.

Rastogi, G., Moin, K., and Abbas, S.M. (2015), "Dimensional analysis and development of similitude rules for dynamic structural models", **5**(3), 68–72.

Ruiz-García, J., Yaghmaei-Sabegh, S., and Bojórquez, E. (2018), "Three-dimensional response of steel moment-resisting buildings under seismic sequences", *Eng. Struct.*, **175**, 399–414. https://doi.org/10.1016/j.engstruct.2018.08.050.

Samanta, A., and Pandey, P. (2018), "Effects of ground motion modification methods and ground motion duration on seismic performance of a 15-storied building", *J. Build. Eng.*, **15**, 14–25. https://doi.org/10.1016/j.jobe.2017.11.003.

Technical information sheet (2018), Suite of Earthquake Tools: Siesmoapps, Seismosoft, Pavia, Italy.

Sooria, S.Z., Sawada, S., and Goto, H. (2012), "Proposal for seismic resistant design in Malaysia: Assessment of possible ground motions in Peninsular Malaysia", *Annuals of Disas. Prev. Res. Inst.*, 55B.

Tan, C.G., Chia, W.T., Majid, T.A., Nazri, F.M., and Adiyanto, M.I., (2017), "Soft storey effects on plastic hinge propagation of moment resisting reinforced concrete building subjected to Ranau earthquake", *AIP Conference Proceedings,* 1892. https://doi.org/10.1063/1.5005748.

Xian, L.J., Lee, L.M., and Yasuo, T. (2017), "Systematic approaches for signal processing of soil shaking table test", *MATEC Web of Conferences*, **138**(04005). https://doi.org/10.1051/matecconf/201713804005.

Yaghmaei-Sabegh, S., Neekmanesha, S., and Ruiz-Garcíab, J. (2017), "Evaluation of approximate methods for estimating maximum displacement response of MDOF systems", *Soil Dynam Earthq. Eng.*, **101**, 125–136. https://doi.org/10.1016/j.soildyn.2017.07.020.

Yaghmaei-Sabegh, S., and Mahdipour-Moghanni, R. (2019), "State-dependent fragility curves using real and artificial earthquake sequences", *Asian J. Civil Eng.*, **20**(4), 619–625. https://doi.org/10.1007/s42107-019-00132-2.

Yaghmaei-Sabegh, S., and Ruiz-García, J. (2016), "Nonlinear response analysis of SDOF systems subjected to doublet earthquake ground motions: A case study on 2012 Varzaghan-Ahar events", *Eng. Struct.*, **110**, 281–292. https://doi.org/10.1016/j.engstruct.2015.11.044.

Yip, C.C., Marsono, A.K., Wong, J.Y., and Lee, S.C. (2018), "Seismic performance of scaled ibs block column for static nonlinear monotonic pushover experimental analysis", *J. Teknologi*, **1**, 89–106.

Yip, C.C., and Marsono, A.K. (2016), "Structural seismic performance of reinforced concrete block system for two storeys safe house", *J. Teknologi*, **2**(78), 83–97.

CC